Discoveries

ORIGINAL RESEARCH COMMUNICATION

p53-PGC-1α Pathway Mediates Oxidative Mitochondrial Damage and Cardiomyocyte Necrosis Induced by Monoamine Oxidase-A Upregulation: Role in Chronic Left Ventricular Dysfunction in Mice

Christelle Villeneuve,[1,2,]* Céline Guilbeau-Frugier,[1,2,]* Pierre Sicard,[1,2] Olivier Lairez,[1,2] Catherine Ordener,[1,2] Thibaut Duparc,[1,2] Damien De Paulis,[3,4] Bettina Couderc,[2] Odile Spreux-Varoquaux,[5] Florence Tortosa,[1,2] Anne Garnier,[6] Claude Knauf,[1,2] Philippe Valet,[1,2] Elisabetta Borchi,[7] Chiara Nediani,[7] Abdallah Gharib,[3,4] Michel Ovize,[3,4] Marie-Bernadette Delisle,[1,2] Angelo Parini,[1,2] and Jeanne Mialet-Perez[1,2]

Abstract

Aims: Oxidative stress and mitochondrial dysfunction participate together in the development of heart failure (HF). mRNA levels of monoamine oxidase-A (MAO-A), a mitochondrial enzyme that produces hydrogen peroxide (H_2O_2), increase in several models of cardiomyopathies. Therefore, we hypothesized that an increase in cardiac MAO-A could cause oxidative stress and mitochondrial damage, leading to cardiac dysfunction. In the present study, we evaluated the consequences of cardiac MAO-A augmentation on chronic oxidative damage, cardiomyocyte survival, and heart function, and identified the intracellular pathways involved. *Results:* We generated transgenic (Tg) mice with cardiac-specific MAO-A overexpression. Tg mice displayed cardiac MAO-A activity levels similar to those found in HF and aging. As expected, Tg mice showed a significant decrease in the cardiac amounts of the MAO-A substrates serotonin and norepinephrine. This was associated with enhanced H_2O_2 generation *in situ* and mitochondrial DNA oxidation. As a consequence, MAO-A Tg mice demonstrated progressive loss of cardiomyocytes by necrosis and ventricular failure, which were prevented by chronic treatment with the MAO-A inhibitor clorgyline and the antioxidant N-acetyl-cystein. Interestingly, Tg hearts exhibited p53 accumulation and downregulation of peroxisome proliferator-activated receptor-γ coactivator-1α (PGC-1α), a master regulator of mitochondrial function. This was concomitant with cardiac mitochondrial ultrastructural defects and ATP depletion. *In vitro*, MAO-A adenovirus transduction of neonatal cardiomyocytes mimicked the results in MAO-A Tg mice, triggering oxidative stress-dependent p53 activation, leading to PGC-1α downregulation, mitochondrial impairment, and cardiomyocyte necrosis. *Innovation and Conclusion:* We provide the first evidence that MAO-A upregulation in the heart causes oxidative mitochondrial damage, p53-dependent repression of PGC-1α, cardiomyocyte necrosis, and chronic ventricular dysfunction. *Antioxid. Redox Signal.* 18, 5–18.

Introduction

HEART FAILURE (HF) IS AMONG the most prevalent diseases in developed countries. Reactive oxygen species (ROS) are believed to play a prominent role in triggering ventricular damage, thus accelerating the progression of HF (10). At the molecular level, chronic exposure to ROS leads to accumulation of oxidized DNA, proteins, and lipids. This results in cardiomyocyte dysfunction and death, a determining factor in ventricular remodelling and failure (8).

[1]INSERM, UMR 1048, Institute of Metabolic and Cardiovascular Diseases, Toulouse, France.
[2]University Paul Sabatier, CHU of Toulouse, Claudius Regaud Institute, 31432 Toulouse, France.
[3]INSERM, U886, University Claude Bernard Lyon 1, 69373 Lyon, France.
[4]Cardiology Department, Louis Pradel Hospital, 69677 Bron, France.
[5]University of Versailles-St-Quentin, Versailles Hospital, 78157 Le Chesnay, France.
[6]INSERM, U-769, University of South-Paris, Chatenay-Malabry, France.
[7]Department of Biochemical Sciences, University of Florence, Florence, Italy.
*These two authors contributed equally to this work.

Innovation

Oxidative stress and mitochondrial dysfunction participate together in the development of heart failure (HF), but the precise source and mechanisms of action are still a matter of debate. In this article, we show for the first time that enhancing monoamine oxidase-A expression, as observed in different models of cardiomyopathy, causes oxidative mitochondrial damage, p53-dependent peroxisome proliferator-activated receptor-γ coactivator-1α (PGC-1α) repression, cardiomyocyte necrosis, and chronic ventricular dysfunction leading to HF.

Mitochondria in cardiomyocytes are at particular risk for oxidative stress (37). To provide energy to meet the high demand, the heart contains numerous mitochondria and is especially vulnerable to mitochondrial dysfunction. Mitochondrial oxidative damage such as DNA mutations have been related to mitochondrial dysfunction, decline in cardiomyocyte function and death (4, 17, 37, 43). In addition, a decrease in energy metabolism in several animal models of HF and in humans has been linked to the downregulation of peroxisome proliferator-activated receptor-γ coactivator-1α (PGC-1α) (32, 33), a master regulator of mitochondrial function that could represent a preferential target for ROS.

Despite accumulative evidence of the deleterious effect of ROS in the failing heart, the precise sources of ROS overproduction remain to be identified. Specific targeting of ROS sources could provide a more effective therapy for HF than global antioxidant therapies, which have given conflicting results in clinical trials (10). Monoamine oxidase-A (MAO-A) is located in the outer mitochondrial membrane of cardiomyocytes and plays a major role in serotonin and catecholamine metabolism (42). MAO-A catalyses the oxidative deamination of monoamines and generates hydrogen peroxide (H_2O_2), aldehyde, and ammonia as by-products (Supplementary Fig. S1A; Supplementary Data are available online at www.liebertpub.com/ars). Thus, MAO-A has been proposed as a relevant source of oxidative stress in the heart. Indeed, a deleterious role for MAO-A/ROS pathway has been demonstrated in acute situations such as ischemia-reperfusion where pharmacological or genetic inactivation of MAO-A prevented cardiomyocyte death (6, 30). In addition, genetic and/or pharmacological inhibition of MAO-A prevented the augmentation of ROS and left ventricular dysfunction in mice with ventricular pressure overload (14).

Interestingly, MAO-A mRNA expression appears to be enhanced in several models of HF (14, 16) as well as in the aging rat heart (24). However, the effect and downstream targets of such chronic increase in MAO-A expression are presently unknown. To address this question, we combined *in vivo* and *in vitro* approaches to analyze the functional consequences of cardiomyocyte MAO-A overexpression using transgenic (Tg) mice and adenoviral-transduced cardiomyocytes.

We found that increasing MAO-A expression to pathophysiological levels observed in failing and aging hearts was sufficient *per se* to cause chronic oxidative stress, mitochondrial damage, and PGC-1α downregulation, thereby contributing to cardiomyocyte necrosis. Consequently, MAO-A Tg mice died prematurely from dilated HF. Interestingly,

we identified for the first time p53 as a major signaling intermediate in H_2O_2-induced mitochondrial damage, PGC-1α downregulation and cardiomyocyte necrosis linked to MAO-A activation.

Results

Myocardial MAO-A activity increases during ventricular hypertrophy, failure and aging

We first analyzed changes in myocardial MAO-A activity in response to various stresses. In a rat model of pressure overload induced by ascendant aortic banding (7), MAO-A activity was significantly increased at the stage of compensated hypertrophy (5 weeks) and decompensated HF (15 weeks), compared to age-matched sham rats (Fig. 1A). Next, we examined the effect of aging on cardiomyocyte MAO-A activity. MAO-A activity increased gradually between 2 and 24 months in cardiac homogenates (Fig. 1B). Interestingly, a profound increase in MAO-A activity was also observed in cardiac myocytes isolated from senescent rats (24-months old) compared to those isolated from 2-months old rats (Fig. 1C).

Tg mice overexpress an active MAO-A enzyme in cardiac mitochondria

In order to mimic changes observed during ventricular pressure overload and aging, we generated mice with cardiomyocyte-specific overexpression of MAO-A under the control of the α-myosin heavy chain (MHC) promoter. Two independent lines of Tg mice were propagated with different levels of MAO-A activity of 9336 ± 2139 pmol/mg/min for Tg 61 and 40291 ± 11912 pmol/mg/min for Tg 113 (Fig. 2A). The levels of MAO-A expression in Tg61 were in the same order of magnitude than those observed in failing and aging hearts (Fig. 1A, B). However, since endogenous MAO-A activity in the mice heart (40 pmol/mg/min) is much lower than in rat heart, the difference observed between Tg61 and nontransgenic (NTg) mice was higher than that observed between pathological and normal rat hearts. The level of MAO-A mRNA overexpression in line 61 was preserved until 6 months (Supplementary Fig. S1B). Western blot analysis demonstrated specific upregulation of MAO-A in cardiac but not liver homogenates compared to NTg littermates (Fig. 2B). In addition, we verified that overexpressed MAO-A was correctly targeted to mitochondria and maintained its catalytic activity. Double immunofluorescence staining on heart sections showed enhanced levels of MAO-A in Tg 61 mice compared to NTg, and colocalization with the mitochondrial protein Cox IV (Fig. 2C). We also found that mitochondria isolated from Tg 61 mice produced greater amounts of H_2O_2 in presence of the MAO substrate tyramine compared to NTg, an effect that was inhibited by 96% with the MAO inhibitor pargyline (Fig. 2D). Finally, we measured by high performance liquid chromatography (HPLC) the levels of MAO-A substrates serotonin (5-hydroxy-tryptamine [5-HT]) and norepinephrine (NE), along with their respective MAO metabolites 5-hydroxyindoleacetic acid (5-HIAA) and dihydroxyphenylglycol (DHPG) in cardiac homogenates. As shown in Figure 2E and F, the ratios of 5-HIAA/5-HT and DHPG/NE were significantly elevated in Tg 61 mice, as a result of both substrate depletion and metabolite accumulation.

FIG. 1. Monoamine oxidase-A (MAO-A) activity is increased in response to hypertrophy, failure, and aging in the heart. (A) MAO-A activity in cardiac homogenates from rats with ascendant aortic banding (Band) for 5 weeks (hypertrophy, $n=5$) or 15 weeks (heart failure [HF], $n=5$) compared to age-matched sham ($n=5$). (B) MAO-A activity in cardiac homogenates from young (2 months), middle age (12 months), and senescent rats (24 months) ($n=6$). (C) MAO-A activity in isolated rat cardiomyocytes at the ages indicated ($n=3$–4). (*$p<0.05$, **$p<0.01$, ***$p<0.001$ vs. indicated value).
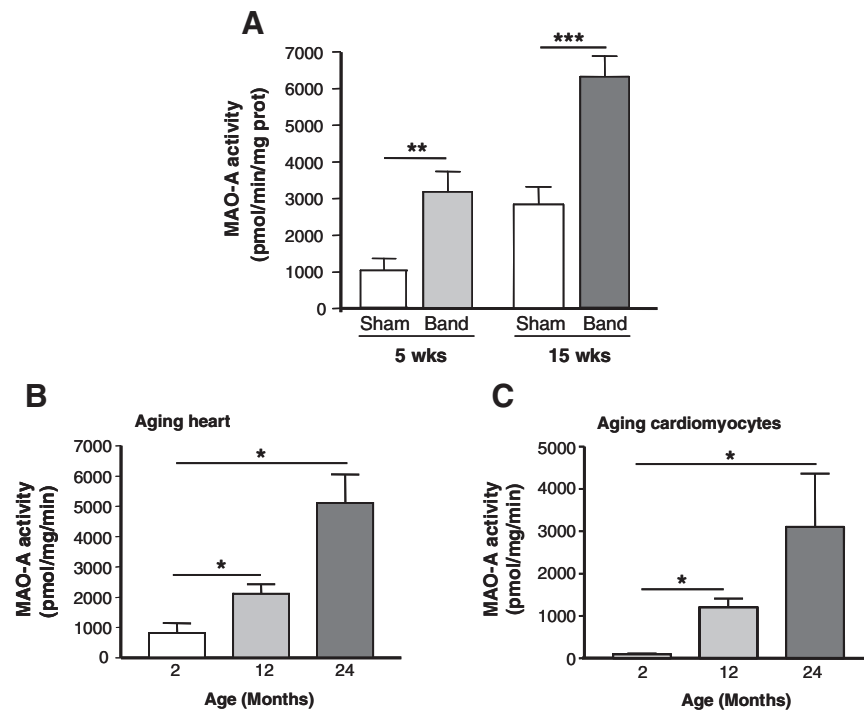
Altogether, our observations demonstrate that oxidative metabolism of 5-HT and NE at the mitochondria is potentiated in MAO-A Tg mice.

MAO-A Tg mice develop dilated cardiomyopathy

To evaluate the consequences of MAO-A upregulation on cardiac morphology and function, echocardiographies were performed in Tg 61 and NTg mice at different ages. Since NTg mice between 3 and 7 months displayed similar morphological parameters, we choose to present only one time-point (3 months) for NTg mice in Table 1. At 1.5 months, ventricular function was not modified in Tg 61 compared to NTg mice (data not shown). However, there was a significant and progressive decrease in fractional shortening (FS) in Tg 61 mice between 3 and 7 months, accompanied by left-ventricular dilatation (Table 1). Myocardial hypertrophy was not observed since neither diastolic septal wall thickness (DSWT) nor posterior wall thickness (PWT) was modified (Table 1). HF was confirmed in 7-month-old Tg mice by a significant increase in lung weight/body weight ratio (7.66 ± 0.47 mg/g vs. 5.41 ± 0.27 mg/g, $p<0.05$) compared to NTg, indicative of pulmonary congestion. As a consequence, life span was severely reduced in Tg 61 mice with a maximum survival around 9 months (Supplementary Fig. S2A). To demonstrate that the deleterious effects of MAO-A upregulation depended on its catalytic activity, we performed echocardiographies on Tg mice treated with the MAO-A inhibitor clorgyline from the age of 1 to 5 months. Chronic administration of clorgyline (10 mg/kg/day) prevented left ventricle (LV) dysfunction and chamber dilatation in Tg mice, compared to untreated Tg mice (Table 1). It is noteworthy that another line of Tg mice (Tg 113), which express a higher amount of MAO-A, shows an accelerated cardiomyopathy, with a dramatic drop in FS at 2 months, ventricular dilatation, and decreased survival (Supplementary Fig. S2A, B). Altogether, our data demonstrate

that an increase in MAO-A catalytic activity induces progressive dilated cardiomyopathy and HF in mice.

Evidence of cell death in the hearts of MAO-A Tg mice, accompanied by inflammatory response, reactive cellular hypertrophy, and fibrosis

To gain more insights into the deleterious effects of myocardial MAO-A upregulation, we performed histological examinations. The most striking feature in Tg hearts was myocardial disarray (Fig. 3A, upper panel). Cardiomyocyte dropout was also evidenced in Tg hearts (Fig. 3A, B), starting around the age of 1.5 months (-17%, nonsignificant), reaching -51% ($p<0.01$) at the age of 3 months and remaining stable until 6 months, compared to NTg mice. As a compensatory response, residual cardiomyocytes were hypertrophied and interstitial fibrosis was enhanced in Tg mice (Fig. 3A, B). Chronic MAO-A inhibition with clorgyline prevented cardiomyocyte dropout, hypertrophy, and fibrosis in Tg mice (Fig. 3A, B). Interestingly, histological findings were recapitulated in Tg 113 mice (Supplementary Fig. S2C). In addition, Tg 61 cardiac mRNA expression analysis confirmed histological findings, with upregulation of pro-inflammatory cytokines as soon as 1.5 months after birth, re-expression of the fetal gene program, and upregulation of extracellular matrix components (Supplementary Fig. S3).

As we found that cardiomyocyte loss occurred between 1.5 and 3 months in Tg mice, we tested for the presence of necrosis and apoptosis to clarify the underlying mechanism of myocyte death at those ages. Regarding necrosis, plasma levels of troponin-I (a sensitive marker of myocyte necrosis) were greatly increased in young Tg mice, while they were undetectable in NTg mice (Fig. 3C). This was in agreement with histological observations at 1.5, 3 (not shown), and 6 months (Fig. 3A, upper panel) that highlighted necrotic areas with disruption of myofibrils, cell debris, loss of nuclei,
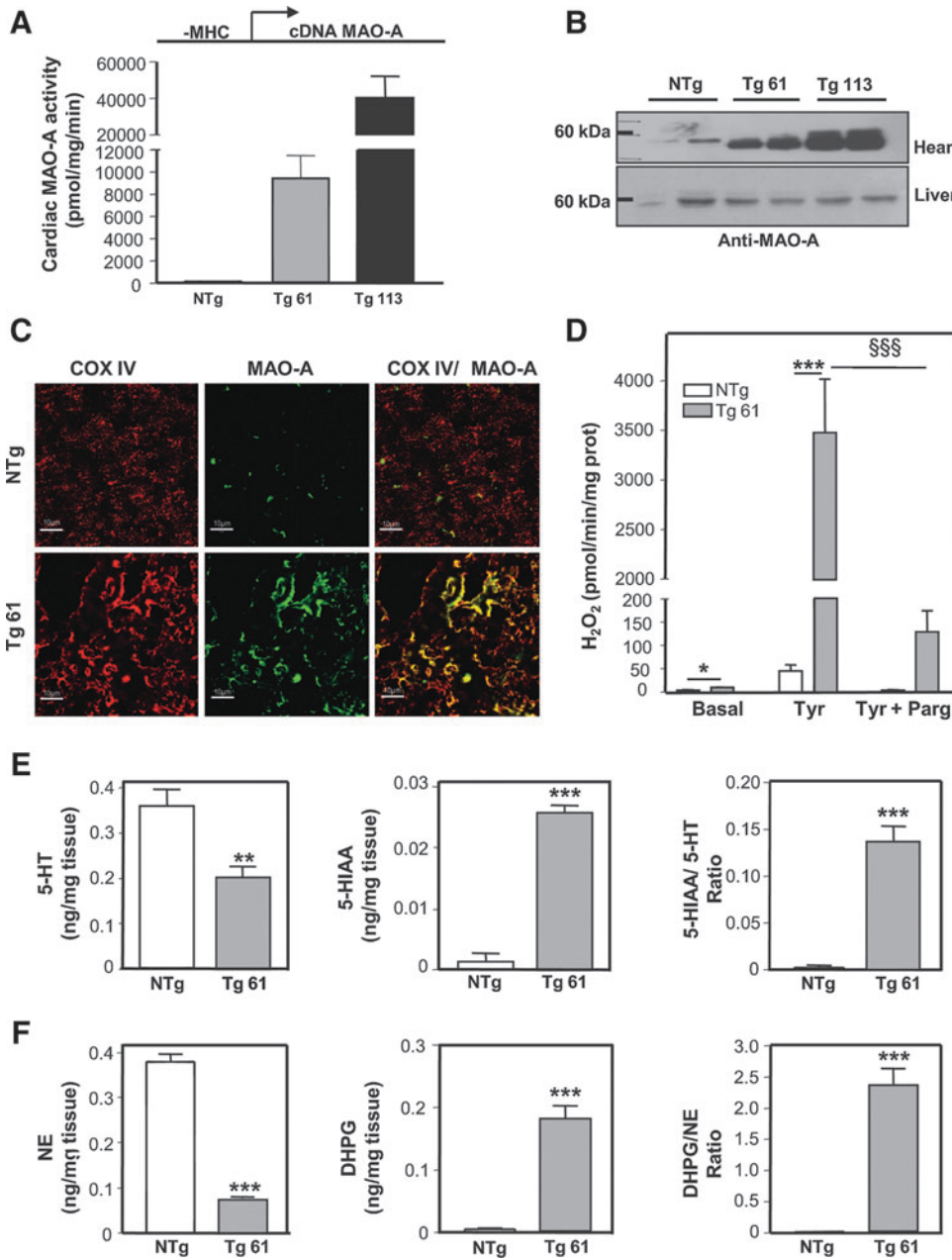
FIG. 2. MAO-A Tg mice overexpress an active MAO-A enzyme, specifically in cardiac mitochondria. (A) Cardiac MAO-A activity in nontransgenic (NTg), transgenic (Tg) 61, and Tg 113 mice at 1.5 months ($n = 3$). The DNA transgene is represented above the histogram, with the α-myosin heavy chain (α-MHC) promoter in front of the MAO-A cDNA. **(B)** Representative MAO-A immunoblot on cardiac and liver homogenates in NTg, Tg 61, and Tg 113 mice. **(C)** Double immunofluorescence staining on heart sections using MAO-A and Cox-IV antibodies ($\times 1000$) at 3 months. **(D)** Hydrogen peroxide (H_2O_2) measurements on isolated cardiac mitochondria incubated with Tyramine ($30\,\mu M$) and pargyline ($100\,\mu M$) ($n = 4$–5) at 3 months. **(E,F)** 5-hydroxytryptamine (5-HT), 5-hydroxyindoleacetic acid (5-HIAA), norepinephrine (NE), and dihydroxyphenylglycol (DHPG) contents in cardiac homogenates from NTg and Tg mice assessed with high performance liquid chromatography ($n = 5$) at 1.5 months ($^*p < 0.05$, $^{**}p < 0.01$, $^{***}p < 0.001$, $^{\S\S\S}p < 0.001$ vs. indicated value).

smudging, and scattered leukocytes in Tg mice (see *arrow* in Fig. 3A). Concerning apoptosis, terminal deoxynucleotidyl transferase dUTP nick end labeling (TUNEL) staining (Fig. 3D) or caspase-3 cleavage (Fig. 3E) were not modified in 1.5-month-old Tg mice. A small increase in the number of apoptotic nuclei was observed at 3 months but did not correlate with caspase-3 activation (not shown). In contrast, the expression of the cell death intermediate p53 was significantly increased in Tg hearts compared to NTg (Fig. 3F) at an early age (1.5 months). As p53 is known to participate, not only in apoptotic but also in necrotic death induction (38, 41), our results suggest that it could be linked to cardiomyocyte necrosis signaling in MAO-A Tg mice. Altogether, although apoptosis cannot be completely excluded, our results point toward cell necrosis as the predominant mechanism for cardiomyocyte dropout in MAO-A-overexpressing mice.

Oxidative stress is increased in hearts from MAO-A Tg mice and participates in the development of dilated cardiomyopathy

First, we evaluated DNA oxidation, a sensitive marker of oxidative stress, in cardiac sections from Tg 61 mice using 8-OH-dG staining. We found that DNA oxidation was significantly increased in Tg hearts compared to NTg hearts as soon as 1.5 months, 3 months (Supplementary Fig. S4A), and 6 months (Fig. 4A). Interestingly, a prominent cytoplasmic staining indicated that mitochondrial DNA was particularly susceptible to oxidation in this model. Chronic treatment of Tg mice with clorgyline prevented accumulation of 8-OH-dG (Fig. 4A). In order to determine whether H_2O_2 was overproduced in Tg 61 mice, we used an H_2O_2-sensitive electrode that detects the concentration of H_2O_2 in ventricles of

TABLE 1. ECHOCARDIOGRAPHIC MEASUREMENTS OF NONTRANSGENIC AND MONOAMINE OXIDASE-A TRANSGENIC
MICE IN CONTROL CONDITIONS AND AFTER CHRONIC TREATMENT WITH CLORGYLINE

	Untreated				Clorgyline-treated		
	NTg	Tg-3 months	Tg-5 months	Tg-7 months	NTg	Tg-3 months	Tg-5 months
No. of animals	16	11	12	4	5	5	5
DSWT, mm	0.67 ± 0.01	0.64 ± 0.01	0.67 ± 0.01	0.68 ± 0.04	0.63 ± 0.01	0.63 ± 0.02	0.66 ± 0.01
DPWT, mm	0.68 ± 0.02	0.64 ± 0.01	0.69 ± 0.02	0.76 ± 0.09	0.67 ± 0.02	0.65 ± 0.02	0.64 ± 0.01
LVEDD, mm	3.84 ± 0.03	4.40 ± 0.09^a	4.50 ± 0.06^a	4.88 ± 0.26^a	3.93 ± 0.16	4.02 ± 0.17	4.16 ± 0.09
LVESD, mm	2.73 ± 0.05	3.40 ± 0.01^a	3.63 ± 0.09^a	4.08 ± 0.39^a	2.74 ± 0.17	2.92 ± 0.18	3.12 ± 0.07^b
FS (%)	28.9 ± 1.0	22.5 ± 1.1^a	19.4 ± 1.2^a	16.5 ± 3.5^a	30.5 ± 2.7	27.1 ± 1.7	25.3 ± 0.7^b
HR, bpm	444.4 ± 12.9	475.0 ± 12.5	457.2 ± 17.0	484.8 ± 30.5	406.5 ± 20.7	453.0 ± 29.1	449.5 ± 8.9

[a]$p < 0.05$ in Tg versus NTg mice.
[b]$p < 0.05$ clorgyline-treated versus untreated age-matched Tg mice.
DSWT, diastolic septal wall thickness; DPWT, diastolic posterior wall thickness; LVEDD, left-ventricular end-diastolic diameter; LVESD, left-ventricular end-systolic diameter; FS, fractional shortening; HR, heart rate assessment by echocardiography; Tg, transgenic; NTg, nontransgenic.

FIG. 3. Evidence of cell death in the hearts of MAO-A Tg mice associated with reactive cellular hypertrophy and fibrosis. (A) Histological characterization (×400) of ventricular pathology by hematoxylin-eosin (HE), periodic acid Schiff (PAS), and Blue Masson's Trichrome staining in cardiac sections of NTg, Tg 61, and clorgyline (Clorg)-treated Tg 61 (Tg 61 + clorg) mice at 5 months. Arrow indicates necrotic area. (B) Quantification of cardiomyocyte number per mm², cardiomyocyte diameter, and collagen content on cardiac sections (n = 5). (C) Evaluation of troponin-I levels by ELISA in plasma from NTg and Tg 61 mice at 1.5 and 3 months (n = 4). (D) Quantification of terminal deoxynucleotidyl transferase dUTP nick end labeling (TUNEL)-positive apoptotic nuclei related to the total number of nuclei in cardiac sections from NTg and Tg 61 mice at 1.5 and 3 months (n = 4). (E) Activated caspase-3 and (F) p53 immunoblots on heart homogenates from NTg and Tg 61 at 1.5 months (*$p < 0.05$, **$p < 0.01$, ***$p < 0.001$, §$p < 0.01$, §§$p < 0.001$ vs. indicated value).
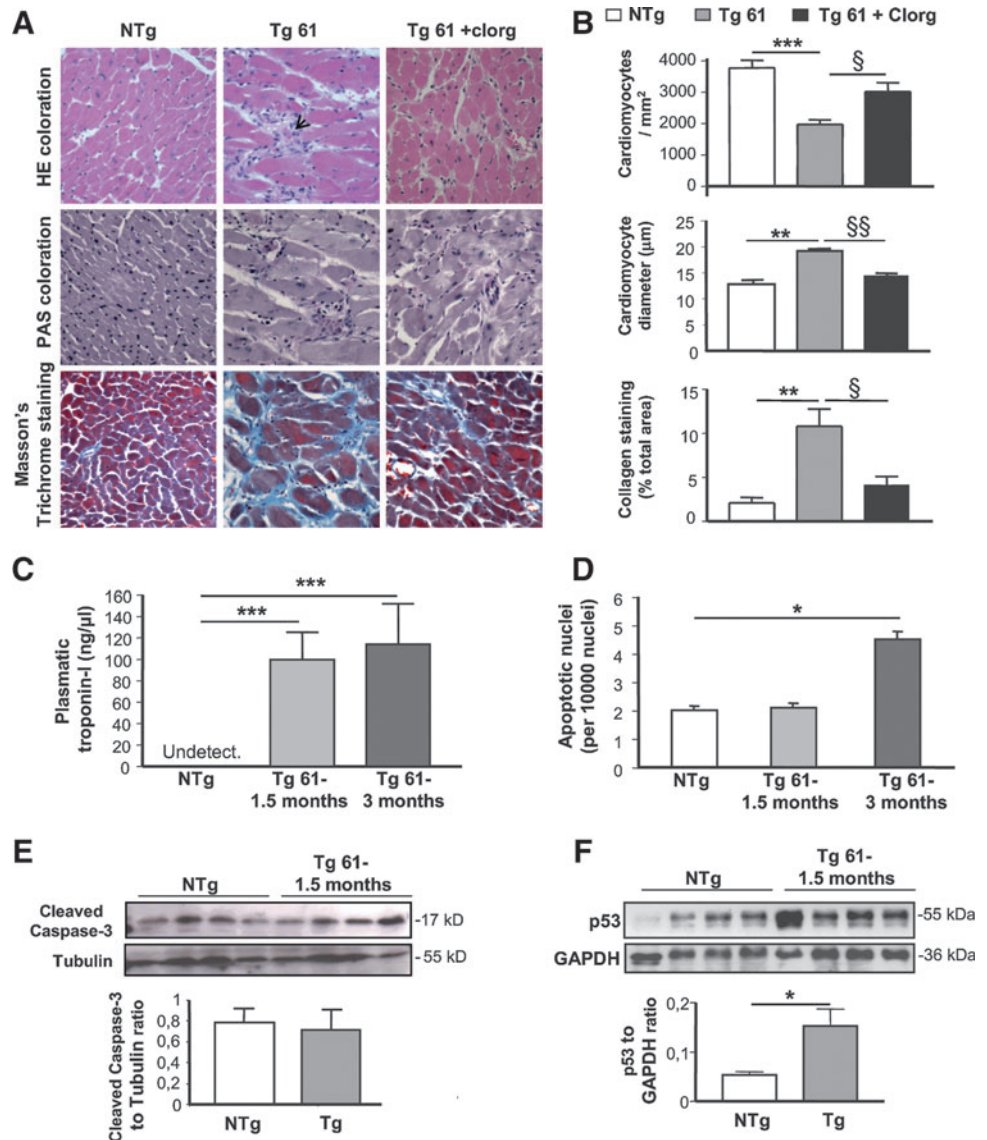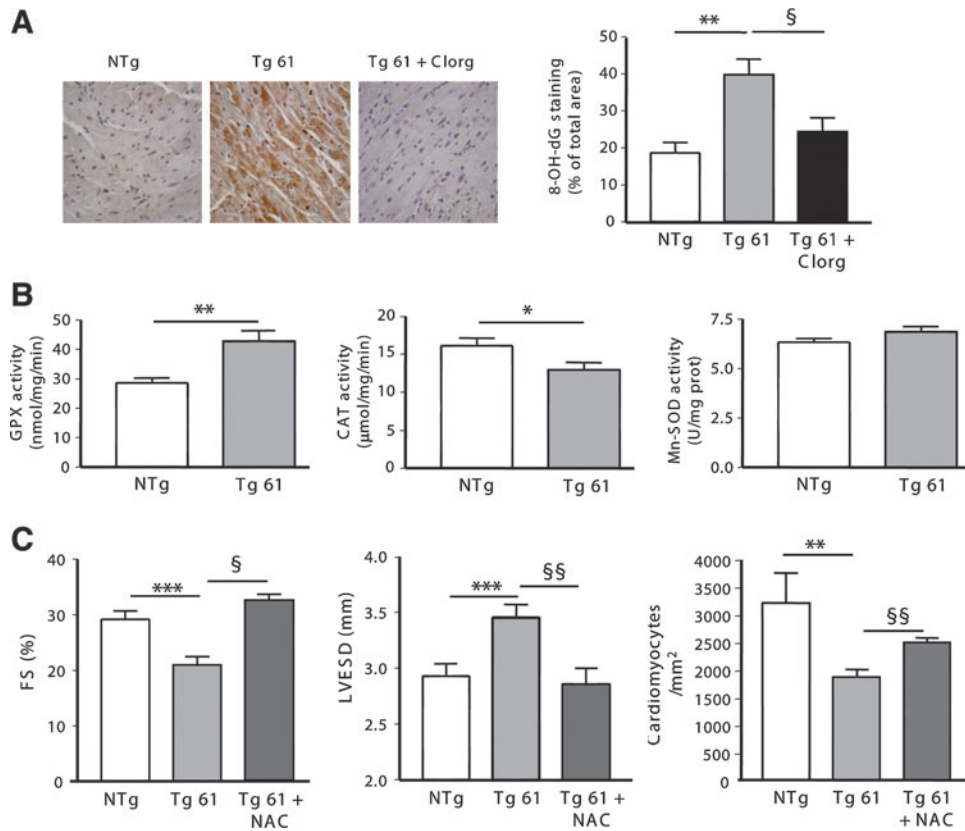
FIG. 4. Oxidative stress is increased in hearts from MAO-A overexpressing mice and participates in the development of dilated cardiomyopathy. **(A)** 8-OH-dG immuno-histochemistry on cardiac sections from 5-month-old NTg, Tg 61, and Clorg-treated Tg 61 (Tg 61+clorg) mice (×400). Quantification of 8-OH-dG staining was expressed as percent of total area ($n = 5$). **(B)** Activity of antioxidant enzymes glutathion peroxidase (GPX), catalase (CAT), and superoxide dismutase (Mn-SOD) in ventricles from 3-month-old NTg and Tg 61 mice ($n = 5$–6). **(C)** Fractional shortening (FS), left-ventricular end-systolic diameter (LVESD), and cardiomyocyte number in 5-month-old NTg, Tg 61-untreated, and N-acetyl-cystein (NAC)-treated Tg 61 (Tg61+NAC) mice ($n = 6$) (*$p < 0.05$, **$p < 0.01$, ***$p < 0.001$, $^{\S}p < 0.05$, $^{\S\S}p < 0.01$ vs. indicated value).

anesthetized mice by an amperometric method. As shown in Supplementary Figure S4B, concentration of H_2O_2 was significantly increased in ventricles from Tg mice at an early age (1.5 months) compared to NTg mice. Then, we analyzed the regulation of antioxidant defenses in cardiac homogenates from NTg and Tg mice. Interestingly, we found that the activity of two enzymes specifically involved in H_2O_2 degradation, glutathion peroxidase (GPX) and catalase (CAT), was modified in Tg mice, while superoxide dismutase (Mn-SOD) activity remained unchanged (Fig. 4B). To evaluate the participation of oxidative stress in the onset of cardiac dysfunction associated with MAO-A upregulation, we used a pharmacological approach with N-acetyl-cystein (NAC), a ROS scavenger. Chronic treatment with 1.5 g/kg/day of NAC from 1 to 6 months improved antioxidant status since it was accompanied by an increase in ventricle gluthatione reduced (GSH) content (Supplementary Fig. S4C). As a consequence, NAC treatment preserved cardiac function (FS) in Tg mice at a level comparable to NTg mice, and prevented cardiac dilatation (left-ventricular end-systolic diameter [LVESD]) (Fig. 4C). Most interestingly, cell loss was also prevented (Fig. 4C). Altogether, our results provide evidence that chronic H_2O_2 generation by MAO-A participates in progressive oxidative damage, cardiomyocyte dropout, and deterioration of cardiac function in Tg mice.

### Upregulation of MAO-A is associated with mitochondrial damage in the heart

Mitochondrial dysfunction plays a major role in HF. Since MAO-A is located in the outer membrane of mitochondria, and mitochondrial DNA is oxidized in Tg mice, we hypothesized that this organelle could be at particular risk for H_2O_2-

mediated injury. Expression profiling using microarrays indicated a global downregulation of genes encoding mitochondrial proteins, and emphasized depressed energy metabolism and oxidative phosphorylation in young Tg mice accompanied by the downregulation of the PGC-1α pathway (Fig. 5A, for a list of genes see Supplementary Tables S1 and S2). Therefore, we examined mitochondrial ultrastructure by electronic microscopy in Tg mice at the age of 1.5 months. In NTg mice, mitochondria were normal with dense matrices filled, homogeneous matrix granules, intact double membrane, and tightly packed cristae (Fig. 5B, *left panel*). In contrast, Tg heart mitochondria tended to make aggregates and were heterogeneous in size (Fig. 5B, *right panel*). In the same cell, small and numerous mitochondria were observed, alternating with normal or swelling mitochondria. The most obvious change was the appearance of electron-lucent areas in mitochondrial matrix and concentric cristae. These morphological features indicated mitochondrial damage. Accordingly, ATP content was decreased in myocardial samples from 1.5-month-old Tg mice, suggesting early impairment in mitochondrial bioenergetics (Fig. 5C). Finally, using real-time reverse transcription–polymerase chain reaction (RT-PCR), we confirmed that expression of PGC-1α, a master regulator of mitochondrial biogenesis, was significantly downregulated in Tg mice at 1.5 months (Fig. 5D).

Upregulation of MAO-A sensitizes cardiomyocytes to necrosis through p53 activation

To gain insight into the mechanism involved in MAO-A-dependent cell necrosis, we developed an *in vitro* model of MAO-A adenoviral vector (AdeMAO-A) transduction in

FIG. 5. MAO-A overexpression induces mitochondrial injury. (A) Geneset Enrichment Analysis for differentially expressed genes by microarray in Tg compared to NTg mice (2 months). Common themes were defined among the various overlapping and unique gene sets. *Blue blocks* and *red blocks* represent highly enriched in category among the various downregulated or upregulated genes, respectively. **(B)** Representative electron micrographs of ventricles from 1.5-month-old NTg and Tg 61 mice (×10,000). Cardiomyocytes from Tg mice show electron-lucent areas in mitochondrial matrix *(arrows)* or concentric cristae *(asterisk)*. **(C)** ATP concentrations in ventricle homogenates at 1.5 months ($n=4$). **(D)** Real-time reverse transcription–polymerase chain reaction (RT-PCR) expression of peroxisome proliferator-activated receptor-γ coactivator-1α (PGC-1α) mRNA at 1.5 months ($n=5$) (*$p<0.05$, **$p<0.01$ *vs.* indicated value).
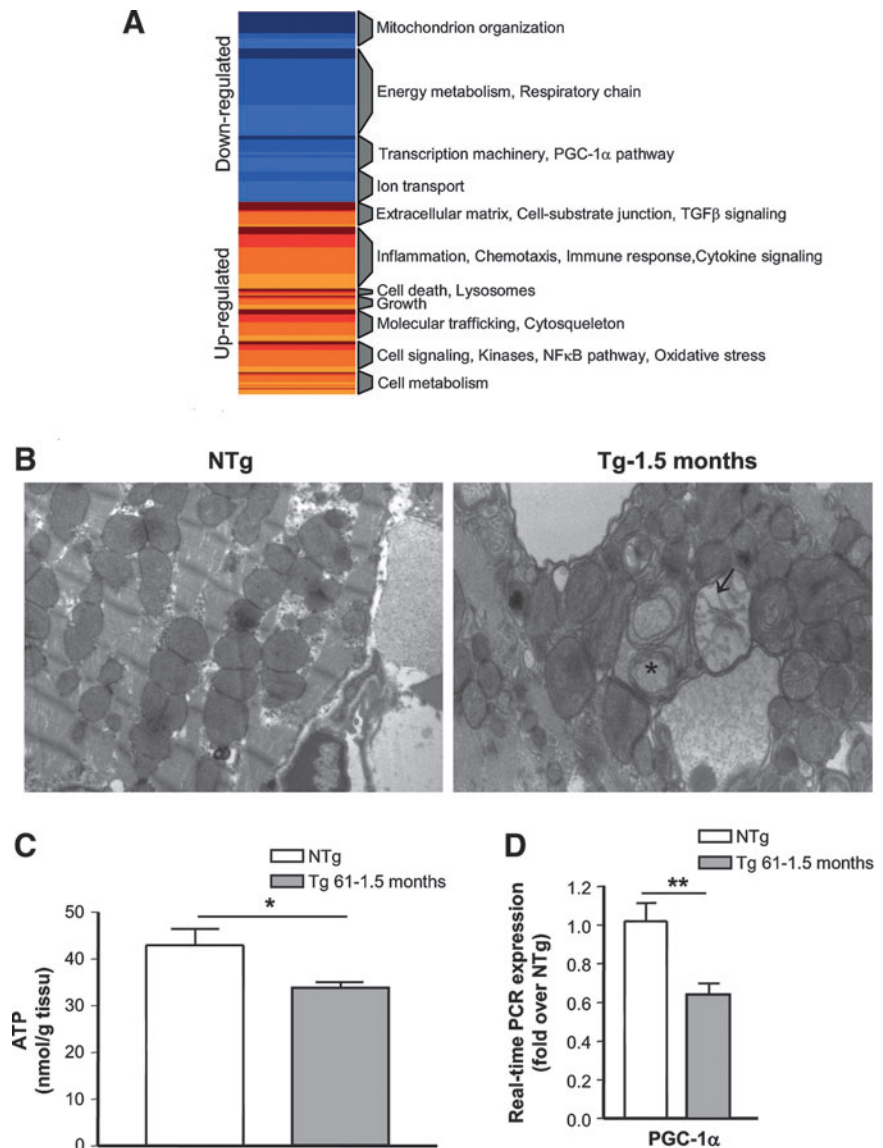
neonatal cardiomyocytes. AdeMAO-A transduction (multiplicity of infection [MOI] 5) induced a significant increase in MAO-A activity in cardiomyocytes (Fig. 6A). Interestingly, application of NE (24 h) induced cardiomyocyte necrosis only in cells transduced with AdeMAO-A, as demonstrated by lactate dehydrogenase (LDH) release (Fig. 6B). Thus, as observed in Tg mice, in the presence of a constant substrate concentration, an increase in MAO-A activity sensitizes cardiomyocytes to necrosis. We confirmed this finding with tyramine, another MAO substrate devoid of membrane receptors in the mammalian heart. Tyramine application for 24 h promoted necrosis in cardiomyocytes transduced with AdeMAO-A (MOI 5), which was prevented by clorgyline and the antioxidants NAC and Trolox (Fig. 6C). Tyramine treatment did not modify MAO-A expression (Supplementary Fig. S5A). Oxidation of the fluorescent probe DCFDA was evidenced 2 h after tyramine application, only in Ade-MAO-A-transduced cardiomyocytes, and was inhibited with clorgyline, NAC, and Trolox (Fig. 6D). In addition, tyramine application decreased GSH content in Ade-MAO-A-transduced cardiomyocytes but not in NAC-treated cardiomyocytes (Sup-

plementary Fig. S5B). As we observed a significant accumulation of p53 in Tg hearts compared to NTg (Fig. 3F), we hypothesized that this protein could play an important role in MAO-A-dependent cell necrosis. We examined the kinetic of p53 activation in AdeMAO-A-transduced cardiomyocytes in the presence of tyramine. Interestingly, tyramine treatment induced a rapid increase in phospho(ser15)-p53 (Fig. 6E), which was dependent on ROS generation since it was prevented in the presence of NAC or Trolox (Fig. 6F). This increase in phospho(ser15)-p53 was not observed in untransduced cardiomyocytes treated with tyramine (Supplementary Fig. S5C). Expression of total p53 was also significantly increased after 6 h of tyramine treatment (Fig. 6E). Therefore, we tested whether p53 activation played a role in MAO-A-dependent necrosis by an siRNA approach. As shown in Figure 6G, p53 siRNA transfection inhibited p53 protein expression at 48 and 72 h compared to Scr-transfected cells. As a consequence, LDH release was significantly reduced in p53-silenced cardiomyocytes compared to Scr (Fig. 6G). Tyramine-induced LDH release was also significantly reduced in cardiomyocytes treated with a pharmacological p53 inhibitor, pifithrin-α, compared to vehicle-treated cardiomyocytes (Fig.
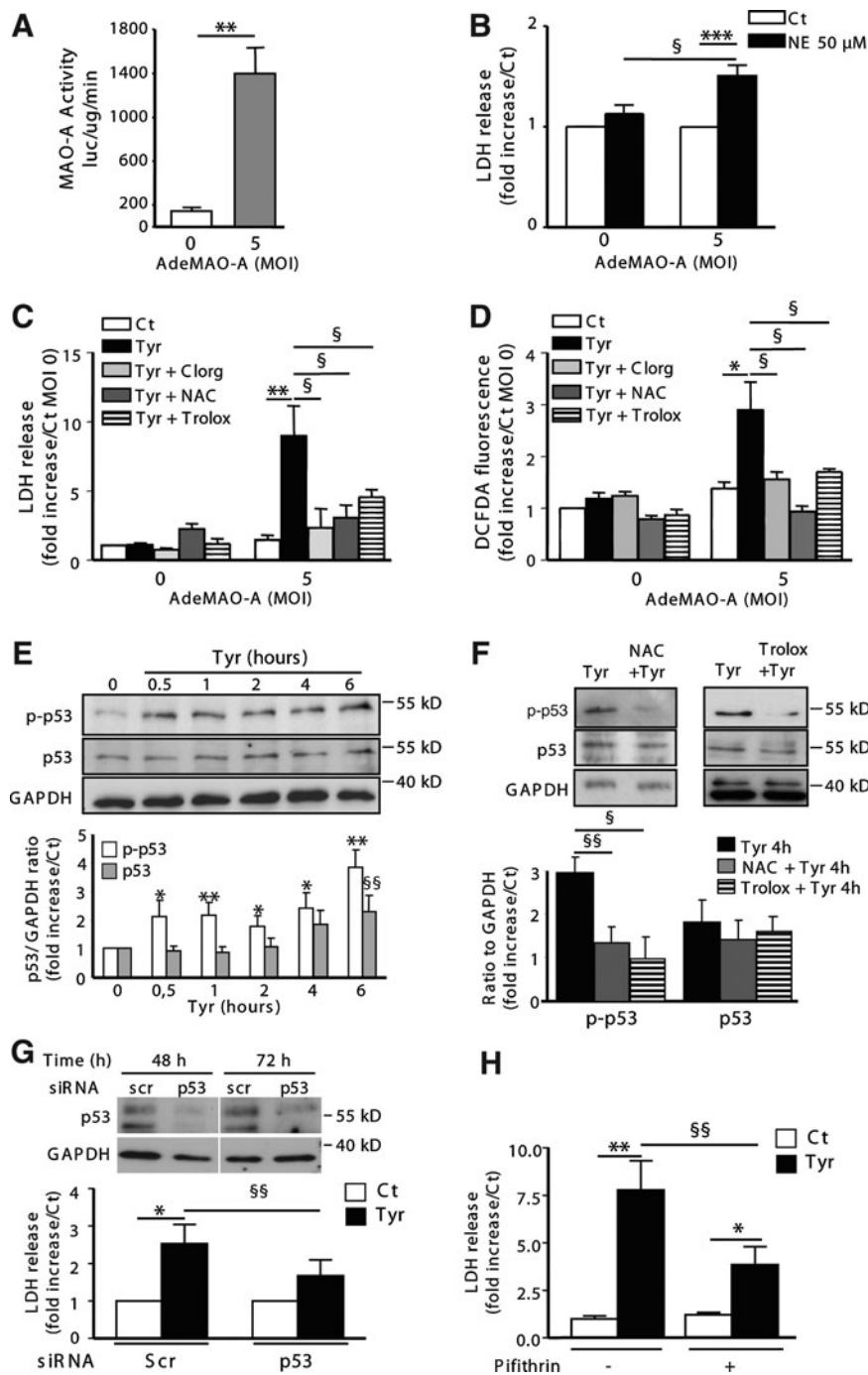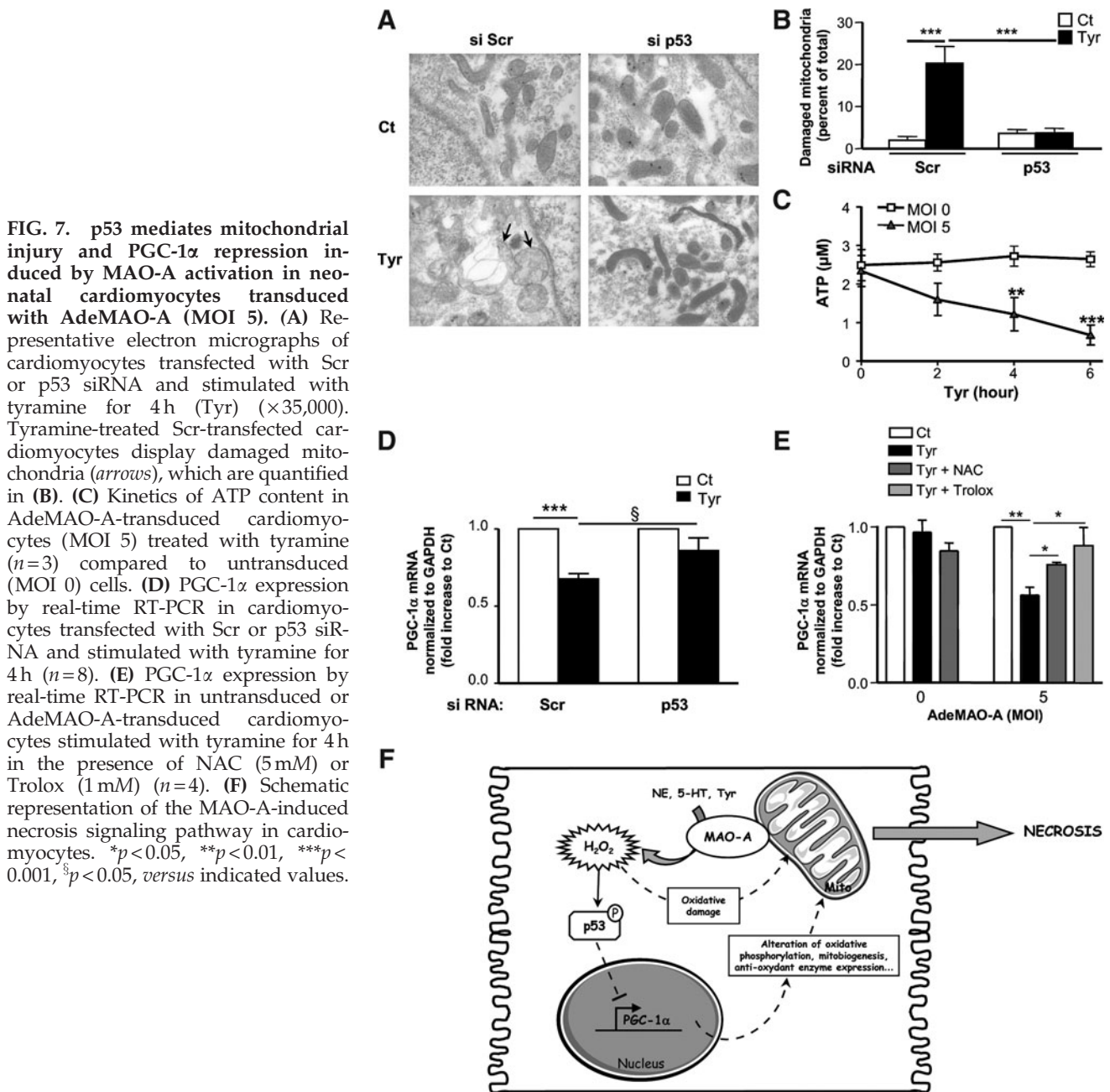
FIG. 6. p53 mediates MAO-A-dependent cardiomyocyte necrosis. (A–D) Neonatal cardiomyocytes were untransduced (multiplicity of infection [MOI] 0) or transduced with Ade-MAO-A at MOI 5. **(A)** Quantification of MAO-A activity by luminescence ($n=3$). **(B)** Lactate dehydrogenase (LDH) release after treatment with $50\,\mu M$ NE for 24 h ($n=8$–9). **(C)** LDH release in response to $500\,\mu M$ tyramine for 24 h in the presence of $10\,\mu M$ Clorg (Tyr + clorg), $5\,mM$ NAC (Tyr + NAC), or $1\,mM$ Trolox (Tyr + Trolox), when indicated ($n=4$–5). **(D)** Reactive oxygen species generation with DCFDA probe in response to $500\,\mu M$ tyramine for 2 h in the presence of NAC ($5\,mM$), Clorg ($10\,\mu M$), or $1\,mM$ Trolox (Tyr + Trolox), when indicated ($n=9$) in untransduced (MOI 0) or AdeMAO-A-transduced (MOI 5) cells. **(E,F)** Analysis of total or phosphor(ser15)-p53 levels by immunoblot in AdeMAO-A-transduced neonatal cardiomyocytes (MOI 5) stimulated with $500\,\mu M$ tyramine for the indicated time in the presence of NAC or Trolox, when indicated ($n=3$–5). GAPDH was used as a loading control. **(G)** LDH release in AdeMAO-A-transduced cardiomyocytes (MOI 5) transfected with Scr or p53 siRNA for 48 h, and stimulated with $500\,\mu M$ tyramine for 24 h ($n=7$). Immunoblot illustrates silencing of p53 protein at 48 and 72 h after siRNA transfection. **(H)** LDH release in AdeMAO-A-transduced cardiomyocytes (MOI 5) stimulated with $500\,\mu M$ tyramine for 24 h in the presence of $20\,\mu M$ pifithrin, when indicated ($n=6$–8) $^*p<0.05$, $^{**}p<0.01$, $^{***}p<0.001$, $^§p<0.05$, $^{§§}p<0.01$ *versus* indicated values or Ct.

6H). In conclusion, our data demonstrate for the first time that p53 activation plays a major role in MAO-A-mediated cardiomyocyte necrosis.

Mitochondrial damage and PGC-1α downregulation are key events in MAO-A-dependent cardiomyocyte necrosis, which are both dependent on p53 activation

Early mitochondrial impairment was observed in MAO-A Tg mice. Thus, we asked whether MAO-A activation could be responsible for mitochondrial damage *in vitro*. As shown in Figure 7A, as soon as 4 h after tyramine application, mitochondrial ultrastructure was severely impaired in AdeMAO-

A-transduced cardiomyocytes but not in untransduced cardiomyocytes (Supplementary Fig. S5D). These ultrastructural alterations fitted with ATP depletion and PGC-1α downregulation, indicating a rapid decline in cell metabolic function in Ade-Mao-A-transduced cardiomyocytes (Fig. 7C, E). Therefore, we asked whether p53 contributed to MAO-A-induced mitochondrial damage. Most interestingly, p53 silencing attenuated mitochondrial ultrastructural defects (Fig. 7A, B) and PGC-1α downregulation (Fig. 7D) compared to Scr-transfected cells. This is consistent with recent data that identified p53 as an important and direct repressor of PGC-1α in the heart, an event that participates in the functional decline of cardiac function during aging (34). Finally, we evaluated

FIG. 7. p53 mediates mitochondrial injury and PGC-1α repression induced by MAO-A activation in neonatal cardiomyocytes transduced with AdeMAO-A (MOI 5). (A) Representative electron micrographs of cardiomyocytes transfected with Scr or p53 siRNA and stimulated with tyramine for 4 h (Tyr) (×35,000). Tyramine-treated Scr-transfected cardiomyocytes display damaged mitochondria (*arrows*), which are quantified in **(B)**. **(C)** Kinetics of ATP content in AdeMAO-A-transduced cardiomyocytes (MOI 5) treated with tyramine (*n*=3) compared to untransduced (MOI 0) cells. **(D)** PGC-1α expression by real-time RT-PCR in cardiomyocytes transfected with Scr or p53 siRNA and stimulated with tyramine for 4 h (*n*=8). **(E)** PGC-1α expression by real-time RT-PCR in untransduced or AdeMAO-A-transduced cardiomyocytes stimulated with tyramine for 4 h in the presence of NAC (5 m*M*) or Trolox (1 m*M*) (*n*=4). **(F)** Schematic representation of the MAO-A-induced necrosis signaling pathway in cardiomyocytes. *$p < 0.05$, **$p < 0.01$, ***$p < 0.001$, §$p < 0.05$, *versus* indicated values.

the contribution of H_2O_2 and oxidative stress in the regulation of PGC-1α. We found that treatment with antioxidants NAC or Trolox prevented PGC-1α mRNA diminution in response to tyramine in MAO-A-overexpressing cardiomyocytes (Fig. 7E). Thus, our results demonstrate that an increase in MAO-A activity sensitizes cardiomyocytes to mitochondrial damage, metabolic decline, and cell necrosis through the generation of oxidative stress. In addition, p53-dependent repression of PGC-1α in cardiomyocytes constitutes an important step in MAO-A-dependent necrosis (Fig. 7F).

Discussion

In the present study, we demonstrate for the first time that a chronic increase in MAO-A engenders mitochondrial oxida-

tive damage, PGC-1α downregulation, myocyte necrosis, and HF. Importantly, we report that p53 acts as a major downstream effector of MAO-A-dependent mitochondrial injury, PGC-1α downregulation, and myocyte necrosis.

A deleterious role for MAO-A/H_2O_2 axis has been well documented in acute situations such as cardiac ischemia-reperfusion. In those studies, pharmacological or genetic inactivation of MAO-A prevented postreperfusion cardiac oxidative stress and cardiomyocyte death (6, 30). However, until now, the importance of MAO-A/H_2O_2 axis in chronic situations such as HF or aging remained poorly understood. Thus, our observation that enhanced MAO-A activity *per se* is sufficient to trigger deleterious effects in the heart represents a new finding, particularly relevant in cardiac diseases where MAO-A upregulation appears to be frequently observed (14,

16). We found that MAO-A activity was increased in rat heart during pressure overload-induced hypertrophy and failure, and during cardiac aging. At present, the rationale for MAO-A upregulation during cardiac stress remains unknown. Sympathetic activation and NE spillover are major features associated with cardiac aging and failure (9, 15). In addition, whole-blood 5-HT levels increase in failing human hearts (28). Therefore, MAO-A upregulation might be an adaptive mechanism to increased levels of substrates, as previously demonstrated in rat mesangial cells (31). However, on the long-term, a chronic increase in 5-HT and catecholamines metabolism by cardiac MAO-A could induce oxidative stress and cardiomyocyte toxicity. Understanding the mechanisms of MAO-A upregulation in the heart seems of major interest and will need to be elucidated in future studies.

In our model, overexpression of MAO-A in mice led to a decrease in cardiac NE and 5-HT, together with an increase in their respective MAO metabolites DHPG and 5-HIAA. This observation is consistent with previous studies showing an accumulation of 5-HT and/or NE levels in the heart after pharmacological or genetic inhibition of MAO-A (14, 19). Monoamine neurotransmitters have major functional implications in the heart, especially in the modulation of cardiac inotropy and compensatory hypertrophy (14, 19). Thus, it is possible that enhanced catabolism of 5-HT and NE in Tg mice contribute to heart dysfunction. On the other hand, monoamine oxidation by MAO-A leads to the generation of H_2O_2, but also aldehyde intermediates, which are rapidly transformed to their corresponding alcohol DHPG and 5-HIAA. Aldehydes are highly reactive species that are toxic for biological systems and may contribute to cell death together with H_2O_2 (22). Although we could not rule out a role for substrate depletion or aldehyde generation in cardiac dysfunction, we provided evidence that oxidative stress played a key role in cardiomyocyte dropout and HF in Tg mice. First, using an original approach of direct real-time H_2O_2 detection in mice heart, we showed that Tg mice were constantly exposed to high H_2O_2 cardiac level at an early age. This observation correlated with the appearance of DNA oxidative damage. Second, chronic treatment with an antioxidant (NAC) increased GSH content and prevented cardiomyocyte death and cardiac failure in Tg mice. Altogether, our results put forward that MAO-A upregulation represents an endogenous system of chronic ROS generation leading to heart dysfunction. This is in accordance with a recent study demonstrating a protective effect of MAO-A inhibition on cardiac oxidative stress and failure during pressure overload (14). Interestingly, we found that the activity of two enzymes involved in H_2O_2 degradation, GPX and CAT, were modified in opposite directions in MAO-A Tg mice. GPX mRNA (not shown) and activity were upregulated, whereas CAT mRNA (not shown) and activity were downregulated. Upregulation of GPX by oxidative stress has been reported in different cell types (21) and may involve the activation of transcription factors such as NFkB or p53 (13), the latter being increased in Tg mice. On the other hand, CAT gene expression has previously been demonstrated to be downregulated by chronic oxidative stress (25, 40). One potential mechanism could involve hypermethylation of the CAT promoter by H_2O_2, which leads to drastic reduction in CAT protein expression (25). Alternatively, inhibition of CAT could be related to the downregulation of PGC-1α in Tg mice, which is a co-factor necessary to maintain

normal expression of antioxidant genes in coordination with FoxO transcription factors (29).

When examining MAO-A-induced cardiomyocyte death, apoptotic nuclei were barely detectable in young Tg mice. Considering that caspase-3 was not activated in Tg hearts, we concluded that such a level of apoptosis was insufficient to explain the major cardiomyocyte loss observed in Tg mice. On the other hand, we found that necrosis was strongly enhanced in Tg hearts, as assessed by histological examinations and plasma troponin-I measurement. Moreover, MAO-A overexpression *in vitro* rendered the cardiomyocytes more vulnerable to necrosis in the presence of NE and tyramine. According to its concentration, H_2O_2 has been demonstrated to induce either apoptosis or necrosis in cardiomyocytes (18). In addition, human aged cells with accumulative oxidative damages are more sensitive to necrosis (26). Therefore, MAO-A upregulation during cardiac failure or aging could sensitize cardiomyocytes to necrosis. This observation is interesting since, after being neglected for a while, necrosis is now recognized as a major way of cell death during chronic HF (27). Hence, elucidating necrotic signaling cascades in the heart seems of major interest. Here, we provide evidence that p53 accumulates in the hearts of Tg mice and can be rapidly activated by tyramine *in vitro*. Both pharmacological and siRNA approaches demonstrated its involvement in cardiomyocyte necrosis induced by MAO-A. The identification of p53 as a mediator of cardiomyocyte necrosis in response to oxidative stress is consistent with accumulating evidence demonstrating an important role of p53 in HF (23, 36). In addition, apart from being a well-known pro-apoptotic factor, p53 has been demonstrated to participate in cell necrosis induced by DNA damage or TNFα (38, 41).

Based on our observations, overexpression of MAO-A *in vitro* and *in vivo* was associated with mitochondrial ultrastructural defects, ATP depletion, and PGC-1α downregulation. *In vitro*, p53 silencing prevented tyramine-induced mitochondrial damage and PGC-1α downregulation, indicating that p53 activation played a key role in amplifying mitochondrial injury in response to MAO-A/H_2O_2. Interestingly, such a link between mitochondrial oxidative damage and p53 activation has been recently observed in a model of HF induced by doxorubicin (39). Downregulation of PGC-1α in our model is interesting since it has been reported to contribute to the maladaptive energetic profile of failing hearts (32). PGC-1α downregulation could alter mitochondrial biogenesis/bioenergetics (3) or lead to a decrease in antioxidant enzymes, as previously described (20).

In conclusion, our results demonstrate that enhancing MAO-A expression, as observed in different models of cardiomyopathy, induces the activation of p53, which acts as a repressor of PGC-1α expression and contributes to bioenergetic defects and mitochondrial damage leading to cardiomyocyte necrosis (Fig. 7F). These findings put forward that an increase in cardiac MAO-A could play a major role in the progression of HF, and propose MAO-A as a promising target for the prevention of cardiomyocyte death in chronic diseases.

Materials and Methods

Generation of Tg mice

The cDNA encoding rat MAO-A (genbank NM_033653) provided by Akio Ito (Kyushu University, Japan) was

subcloned into the full-length mouse α-MHC promoter. Briefly, a 2060-bp cDNA, including 6 bp of the 5′ and 474 bp of the 3′ flanking sequences, was subcloned into the *Sal*I site of the polylinker of the α-MHC promoter construct (12). The resulting recombinant plasmid, pαMHC-MAO-A, was confirmed by restriction mapping and nucleotide sequencing. A linear 8000-bp DNA fragment was microinjected into fertilized eggs at the "Institut Clinique de la Souris" (Strasbourg, France). Offsprings were genotyped and founders were bred with C57BL6/J mice to establish stable Tg mice. Mice were housed in a pathogen-free facility and handled in accordance with the principles and procedures outlined in Council Directive 86/609/EEC. For all experiments, littermates were used as controls.

Assays of MAO activity

MAO-A activities in cardiac tissues were performed as previously described (19). For *in vitro* assays, 5 μg of cellular lysates was incubated with 20 μM MAO-A substrate (MAO-Glo Assay kit; Promega) for 20 min at 37°C and nonspecific activity was defined in the presence of clorgyline.

Primary cultures of cardiomyocytes

Adult ventricular myocytes were obtained from hearts of male Sprague-Dawley rats at the ages of 2, 12, and 24 months with retrograde perfusion, as previously described (6). For neonatal cardiomyocytes, hearts of 2–3-day-old Sprague-Dawley rats were dissociated with collagenase type II, 0.1% (Biovalley), as previously described (30). Myocyte enrichment was performed by centrifugation through a discontinuous Percoll gradient and resultant suspension of myocytes was plated onto gelatin-coated culture dishes. About 24 h after adenovirus transduction, the medium was replaced with the Ham-F12 medium supplemented with dialyzed-FCS 3% and inhibitors (clorgyline, NAC, pifithrin-α), when indicated. Tyramine was added 2 h later for the indicated time. The selected siRNA for p53 is an ON-TARGET plus SMART pool siRNA (Dharmacon). SiRNAs were transfected 24 h before AdeMAO-A adenovirus transduction, using the Dharmafect reagent according to the manufacturer's recommendations.

Western blot

Ventricular homogenates and cardiomyocyte extracts were electrophoresed and transferred as described (19). Membranes were incubated with anti-MAO-A, anti-GAPDH antibodies (Santa Cruz Biotechnology) or anti-caspase-3, anti-p53, anti-phospho-p53 antibodies (Cell Signaling).

Immunofluorescence

Frozen cardiac sections were fixed with PFA 3% for 15 min and neutralized with glycine 100 m*M*. After permeabilization with Triton 0.5%, heart sections were incubated first with MAO-A antibody overnight at 4°C, and cytochrome c oxidase IV (CoxIV) antibody (Santa Cruz Biotechnology) at room temperature for 1 h. After washing, sections were incubated for 1 h at room temperature with Oregon Green 488-conjugated goat antirabbit or Alexa 594-conjugated goat antimouse antibodies (Invitrogen). Images were acquired using a DM600 microscope (Leica) fitted with a Roper COOLsnap ES CCD camera. Images were denoized using the

Nearest Neighbours approach of the 2D Deconvolution setup of Metamorph software (Filter size: 2; Scaling Factor: 0.5; Result Scale: 2).

Electron microscopy

LVs of mice were cut in cubes of $1 \, mm^3$ and placed in glutaraldehyde 2.5%. Semi-thin (1 μm) sections were stained with toluidine blue. Trimmed ultra-thin sections (600 Å) were stained with uranyl acetate and lead citrate. Sections were examined under a transmission electron microscopy (Hitashi 5HU12A).

Mitochondrial H_2O_2 production

Cardiac mitochondria were isolated using the procedure of Gomez *et al.* (11). Total H_2O_2 production was measured using a fluorimeter F-2500 (Hitachi) and a fluorescent probe Amplex Red® (10 μM) in the presence of 0.6 U/ml horseradish peroxidase (excitation and emission wavelengths set to 530 and 590 nm, respectively).

Assays of 5-HT, 5-HIAA, NE, and DHPG

Snap-frozen ventricular tissues were homogeneously grinded in 1.5 ml water. Assays for 5-HT, 5-HIAA (2), and NE, DHPG (5) were performed using two different HPLC methods with coulometric detection applied to tissues. For 5-HT and 5-HIAA, determinations were made without extraction on the centrifugated supernatants after deproteinization of the aqueous mixture using $HClO_4$ 0.1 *M* and ascorbic acid 3.10^{-4} *M*. For NE and DHPG determinations, 500 μl samples of the aqueous centrifugated mixture were extracted using acid-washed alumina columns.

Echocardiography

Animals were anesthetized with 2% isoflurane and examined with noninvasive echocardiography (echocardiograph Vivid 7 ultrasound; GE). Cardiac ventricular dimensions were measured on M-mode images at least five times for the number of animals indicated.

Histological analysis

Ventricles were incubated in the Carnoy's fixative solution (ethanol 60%, chloroform 30%, and acetic acid 10%), embedded in paraffin, and transversally sectioned. Five-μm tissue sections were stained with H&E, Masson's Trichrome, or PAS. Fibrosis was measured as positively stained area with Masson's Trichrome (green), and expressed as percent of total area, using a computer-based morphometric analysis (Nis-element; Nikon). Cardiomyocyte diameter was evaluated after coloration with PAS (250–300 cells counted per heart) on LV. Number of cardiomyocytes per total myocardial area was measured using manual-counting function of the analysis software in three consecutive areas of the LV. For 8-OH-dG (a marker of nuclear and mitochondrial DNA oxidation) immunohistochemistry, antigen retrieval was performed using citrate solution (sodium citrate 1 *M*, citric acid 1 *M*, pH 6.0) at 97°C during 40 min. After washing with deionized water, endogenous peroxidase activity was blocked with H_2O_2 30% for 10 min. 8-OH-dG mouse monoclonal antibody (1:200; AbCys) was incubated for 2 h at 37°C and secondary antibody for 30 min at room temperature. Slides were washed and

incubated with 1:50 DAB in substrate buffer for 5 min, and then counterstained with 1:4 Mayer's hematoxylin. Positively stained area was quantified using a computer-based morphometric analysis (Nis-element; Nikon) and calculated as percent of total area. Apoptosis was evaluated by TUNEL staining on cardiac sections as previously described (6).

Real-time RT-PCR

Extraction of RNA from cardiac ventricles was performed using column affinity purification (Qiagen). cDNAs were synthesized using the superscript II RT-PCR system (Invitrogen) with random hexamers. Real-time PCR was performed on a StepOnePlus system (Applied Biosystem) in 96-well plates with specific primers and SYBR green mix (Eurogentec). The primers were as followed—mouse PGC-1α-F: ACGGTTTACATGAACACAGCTGC, mouse PGC-1α-R: CTTGTTCGTTCTGTTCAGGTGC, rat PGC-1α-F: CACCAAA CCCACAGAGAACAG, and rat PGC-1α-R: GCAGTTCCAG AGAGTTCCACA.

Plasmatic troponin

Plasmatic troponin-I was detected using an ELISA kit according to the manufacturer's instructions (Life Diagnostic). Briefly, plasma samples were incubated for 1 h at room temperature with an HRP-conjugated anti-cTn-I antibody in microtiter wells. After extensive wash, HRP substrate was added in each well for 20 min at room temperature and the reaction stopped with HCl 1 M. Absorbance was measured at 450 nm and plasmatic cTn-I concentration was determined using cTn-I standards.

Antioxidant enzyme activities

CAT activity was determined by the procedure of Aebi (1). For GPX and Mn-SOD, activities were evaluated as previously described (35).

Microarray analysis

Total RNA was prepared as described above. The quality of samples was verified with Agilent Bioanalyzer 6000 (Agilent Technologies). Hybridization of RNA was done on Agilent Mouse Genome CGH 44K chip at the Genotoul Biopuces Plate-forme). Raw data (median values) were normalized and processed using the R statistical software and the limma package for microarrays. Weights were attributed to flag bad data points and the remaining values were Loess-normalized within arrays and quantile-normalized between arrays. Limma was used to generate log2 ratios (coefficents) and p-values (using eBayes) in order to select genes with differential expression between groups that were also well behaved in terms of expression within each individual group. Using a log2 ratio of 0.5 (fold-change 1.4) and a p-value cutoff of 0.005, genes were selected for analysis. GeneSet Enrichment Analysis for categorical feature overrepresentation in each gene list (upregulated or downregulated) was performed using Toppgene (http://toppgene.cchmc.org/). For each enriched Geneset, the enrichment p-value for nonrandom list intersection (using Bonferroni p-value correction) was converted to a significance score [$S = -\log (pval)$] and a matrix was constructed with colors scaled to significance scores. Common themes were defined among the various overlapping and unique Genesets.

ATP measurement

Snap-frozen cardiac samples (30 mg) were homogenized in 500-μl ice-cold perchloric acid (10% v/v), sited on ice for 10 min, and centrifuged at 14,000 rpm for 10 min at 4°C. Supernatants were neutralized with KOH 2.5 M and centrifuged at 4500 rpm for 5 min. Supernatants from cardiac sample extraction or cell lysates were assayed for ATP assay kit (Bioluminescence assay kit HS II; Roche).

Adenoviral constructs

Replication-deficient (ΔE1, E3), adenoviral vector-expressing, MAO-A-coding region (1.9 kb) under the control of the CMV promoter was constructed with the AdEasy System (Qbiogen). Replication-defective MAO-A adenovirus (Ade-MAO-A) was generated by transfection of 293A cells with a single isolate of recombinant adenoviral vector, expanded, and purified. Viral titers were initially determined by optical absorbance at 260 nm. Infections were done at a certain MOI based on this definition; for example, 1×10^6 bav/1×10^6 cells = MOI 1.

Intracellular ROS measurement

Generation of ROS in cardiomyocytes was evaluated using DCFDA probe as previously described (6).

LDH release assay

For quantitative assessment of cardiomyocyte necrosis, LDH release in culture medium was measured using LDH-cytotoxicity Assay Kit according to the manufacturer's instructions (Biovision).

Statistical analysis

Results are expressed as mean ± SEM. Experimental groups were compared using Student's t-test or one-way analysis of variance, as appropriate. A value of $p < 0.05$ was considered significant.

Acknowledgments

Author Disclosure Statement

No competing financial interests exist.

References

1. Aebi H. Catalase *in vitro*. *Methods Enzymol* 105: 121–126, 1984.
2. Alvarez JC, Bothua D, Collignon I, Advenier C, and Spreux-Varoquaux O. Simultaneous measurement of dopamine, serotonin, their metabolites and tryptophan in mouse brain homogenates by high-performance liquid chromatography

with dual coulometric detection. *Biomed Chromatogr* 13: 293–298, 1999.

3. Arany Z, He H, Lin J, Hoyer K, Handschin C, Toka O, Ahmad F, Matsui T, Chin S, Wu PH, Rybkin, II, Shelton JM, Manieri M, Cinti S, Schoen FJ, Bassel-Duby R, Rosenzweig A, Ingwall JS, and Spiegelman BM. Transcriptional coactivator PGC-1 alpha controls the energy state and contractile function of cardiac muscle. *Cell Metab* 1: 259–271, 2005.

4. Barja G and Herrero A. Oxidative damage to mitochondrial DNA is inversely related to maximum life span in the heart and brain of mammals. *FASEB J* 14: 312–318, 2000.

5. Berlin I, Said S, Spreux-Varoquaux O, Olivares R, Launay JM, and Puech AJ. Monoamine oxidase A and B activities in heavy smokers. *Biol Psychiatry* 38: 756–761, 1995.

6. Bianchi P, Kunduzova O, Masini E, Cambon C, Bani D, Raimondi L, Seguelas MH, Nistri S, Colucci W, Leducq N, and Parini A. Oxidative stress by monoamine oxidase mediates receptor-independent cardiomyocyte apoptosis by serotonin and postischemic myocardial injury. *Circulation* 112: 3297–3305, 2005.

7. De Sousa E, Veksler V, Minajeva A, Kaasik A, Mateo P, Mayoux E, Hoerter J, Bigard X, Serrurier B, and Ventura-Clapier R. Subcellular creatine kinase alterations. Implications in heart failure. *Circ Res* 85: 68–76, 1999.

8. Dorn GW, 2nd. Apoptotic and non-apoptotic programmed cardiomyocyte death in ventricular remodelling. *Cardiovasc Res* 81: 465–473, 2009.

9. Eisenhofer G, Friberg P, Rundqvist B, Quyyumi AA, Lambert G, Kaye DM, Kopin IJ, Goldstein DS, and Esler MD. Cardiac sympathetic nerve function in congestive heart failure. *Circulation* 93: 1667–1676, 1996.

10. Giordano FJ. Oxygen, oxidative stress, hypoxia, and heart failure. *J Clin Invest* 115: 500–508, 2005.

11. Gomez L, Paillard M, Thibault H, Derumeaux G, and Ovize M. Inhibition of GSK3beta by postconditioning is required to prevent opening of the mitochondrial permeability transition pore during reperfusion. *Circulation* 117: 2761–2768, 2008.

12. Gulick J, Subramaniam A, Neumann J, and Robbins J. Isolation and characterization of the mouse cardiac myosin heavy chain genes. *J Biol Chem* 266: 9180–9185, 1991.

13. Hussain SP, Amstad P, He P, Robles A, Lupold S, Kaneko I, Ichimiya M, Sengupta S, Mechanic L, Okamura S, Hofseth LJ, Moake M, Nagashima M, Forrester KS, and Harris CC. p53-induced up-regulation of MnSOD and GPx but not catalase increases oxidative stress and apoptosis. *Cancer Res* 64: 2350–2356, 2004.

14. Kaludercic N, Takimoto E, Nagayama T, Feng N, Lai EW, Bedja D, Chen K, Gabrielson KL, Blakely RD, Shih JC, Pacak K, Kass DA, Di Lisa F, and Paolocci N. Monoamine oxidase A-mediated enhanced catabolism of norepinephrine contributes to adverse remodeling and pump failure in hearts with pressure overload. *Circ Res* 106: 193–202, 2010.

15. Kaye D and Esler M. Sympathetic neuronal regulation of the heart in aging and heart failure. *Cardiovasc Res* 66: 256–264, 2005.

16. Kong SW, Bodyak N, Yue P, Liu Z, Brown J, Izumo S, and Kang PM. Genetic expression profiles during physiological and pathological cardiac hypertrophy and heart failure in rats. *Physiol Genomics* 21: 34–42, 2005.

17. Kujoth GC, Hiona A, Pugh TD, Someya S, Panzer K, Wohlgemuth SE, Hofer T, Seo AY, Sullivan R, Jobling WA, Morrow JD, Van Remmen H, Sedivy JM, Yamasoba T, Tanokura M, Weindruch R, Leeuwenburgh C, and Prolla TA.

18. Mitochondrial DNA mutations, oxidative stress, and apoptosis in mammalian aging. *Science* 309: 481–484, 2005.

18. Kwon SH, Pimentel DR, Remondino A, Sawyer DB, and Colucci WS. H(2)O(2) regulates cardiac myocyte phenotype via concentration-dependent activation of distinct kinase pathways. *J Mol Cell Cardiol* 35: 615–621, 2003.

19. Lairez O, Calise D, Bianchi P, Ordener C, Spreux-Varoquaux O, Guilbeau-Frugier C, Escourrou G, Seif I, Roncalli J, Pizzinat N, Galinier M, Parini A, and Mialet-Perez J. Genetic deletion of MAO-A promotes serotonin-dependent ventricular hypertrophy by pressure overload. *J Mol Cell Cardiol* 46: 587–595, 2009.

20. Lu Z, Xu X, Hu X, Fassett J, Zhu G, Tao Y, Li J, Huang Y, Zhang P, Zhao B, and Chen Y. PGC-1 alpha regulates expression of myocardial mitochondrial antioxidants and myocardial oxidative stress after chronic systolic overload. *Antioxid Redox Signal* 13: 1011–1022, 2010.

21. Lubos E, Loscalzo J, and Handy DE. Glutathione peroxidase-1 in health and disease: from molecular mechanisms to therapeutic opportunities. *Antioxid Redox Signal* 15: 1957–1997, 2011.

22. Marchitti SA, Deitrich RA, and Vasiliou V. Neurotoxicity and metabolism of the catecholamine-derived 3,4-dihydroxyphenylacetaldehyde and 3,4-dihydroxyphenylglycolaldehyde: the role of aldehyde dehydrogenase. *Pharmacol Rev* 59: 125–150, 2007.

23. Matsusaka H, Ide T, Matsushima S, Ikeuchi M, Kubota T, Sunagawa K, Kinugawa S, and Tsutsui H. Targeted deletion of p53 prevents cardiac rupture after myocardial infarction in mice. *Cardiovasc Res* 70: 457–465, 2006.

24. Maurel A, Hernandez C, Kunduzova O, Bompart G, Cambon C, Parini A, and Frances B. Age-dependent increase in hydrogen peroxide production by cardiac monoamine oxidase A in rats. *Am J Physiol Heart Circ Physiol* 284: H1460–H1467, 2003.

25. Min JY, Lim SO, and Jung G. Downregulation of catalase by reactive oxygen species via hypermethylation of CpG island II on the catalase promoter. *FEBS Lett* 584: 2427–2432.

26. Miyoshi N, Oubrahim H, Chock PB, and Stadtman ER. Age-dependent cell death and the role of ATP in hydrogen peroxide-induced apoptosis and necrosis. *Proc Natl Acad Sci U S A* 103: 1727–1731, 2006.

27. Nakayama H, Chen X, Baines CP, Klevitsky R, Zhang X, Zhang H, Jaleel N, Chua BH, Hewett TE, Robbins J, Houser SR, and Molkentin JD. Ca2 + - and mitochondrial-dependent cardiomyocyte necrosis as a primary mediator of heart failure. *J Clin Invest* 117: 2431–2444, 2007.

28. Nigmatullina RR, Kirillova VV, Jourjikiya RK, Mukhamedyarov MA, Kudrin VS, Klodt PM, and Palotas A. Disrupted serotonergic and sympathoadrenal systems in patients with chronic heart failure may serve as new therapeutic targets and novel biomarkers to assess severity, progression and response to treatment. *Cardiology* 113: 277–286, 2009.

29. Olmos Y, Valle I, Borniquel S, Tierrez A, Soria E, Lamas S, and Monsalve M. Mutual dependence of Foxo3a and PGC-1alpha in the induction of oxidative stress genes. *J Biol Chem* 284: 14476–14484, 2009.

30. Pchejetski D, Kunduzova O, Dayon A, Calise D, Seguelas MH, Leducq N, Seif I, Parini A, and Cuvillier O. Oxidative stress-dependent sphingosine kinase-1 inhibition mediates monoamine oxidase A-associated cardiac cell apoptosis. *Circ Res* 100: 41–49, 2007.

31. Pizzinat N, Marchal-Victorion S, Maurel A, Ordener C, Bompart G, and Parini A. Substrate-dependent regulation of

MAO-A in rat mesangial cells: involvement of dopamine D2-like receptors. *Am J Physiol Renal Physiol* 284: F167–F174, 2003.

32. Rimbaud S, Garnier A, and Ventura-Clapier R. Mitochondrial biogenesis in cardiac pathophysiology. *Pharmacol Rep* 61: 131–138, 2009.

33. Rosca MG and Hoppel CL. Mitochondria in heart failure. *Cardiovasc Res* 88: 40–50, 2010.

34. Sahin E, Colla S, Liesa M, Moslehi J, Muller FL, Guo M, Cooper M, Kotton D, Fabian AJ, Walkey C, Maser RS, Tonon G, Foerster F, Xiong R, Wang YA, Shukla SA, Jaskelioff M, Martin ES, Heffernan TP, Protopopov A, Ivanova E, Mahoney JE, Kost-Alimova M, Perry SR, Bronson R, Liao R, Mulligan R, Shirihai OS, Chin L, and DePinho RA. Telomere dysfunction induces metabolic and mitochondrial compromise. *Nature* 470: 359–365, 2011.

35. Sebastiani M, Giordano C, Nediani C, Travaglini C, Borchi E, Zani M, Feccia M, Mancini M, Petrozza V, Cossarizza A, Gallo P, Taylor RW, and d'Amati G. Induction of mitochondrial biogenesis is a maladaptive mechanism in mitochondrial cardiomyopathies. *J Am Coll Cardiol* 50: 1362–1369, 2007.

36. Toko H, Takahashi H, Kayama Y, Oka T, Minamino T, Okada S, Morimoto S, Zhan DY, Terasaki F, Anderson ME, Inoue M, Yao A, Nagai R, Kitaura Y, Sasaguri T, and Komuro I. Ca2 + /calmodulin-dependent kinase IIdelta causes heart failure by accumulation of p53 in dilated cardiomyopathy. *Circulation* 122: 891–899, 2010.

37. Tsutsui H, Kinugawa S, and Matsushima S. Mitochondrial oxidative stress and dysfunction in myocardial remodelling. *Cardiovasc Res* 81: 449–456, 2009.

38. Tu HC, Ren D, Wang GX, Chen DY, Westergard TD, Kim H, Sasagawa S, Hsieh JJ, and Cheng EH. The p53-cathepsin axis cooperates with ROS to activate programmed necrotic death upon DNA damage. *Proc Natl Acad Sci U S A* 106: 1093–1098, 2009.

39. Velez JM, Miriyala S, Nithipongvanitch R, Noel T, Plabplueng CD, Oberley T, Jungsuwadee P, Van Remmen H, Vore M, and St Clair DK. p53 Regulates oxidative stress-mediated retrograde signaling: a novel mechanism for chemotherapy-induced cardiac injury. *PLoS One* 6: e18005, 2011.

40. Venkatesan B, Mahimainathan L, Das F, Ghosh-Choudhury N, and Ghosh Choudhury G. Downregulation of catalase by reactive oxygen species via PI 3 kinase/Akt signaling in mesangial cells. *J Cell Physiol* 211: 457–467, 2007.

41. Waters FJ, Shavlakadze T, McIldowie MJ, Piggott MJ, and Grounds MD. Use of pifithrin to inhibit p53-mediated signalling of TNF in dystrophic muscles of mdx mice. *Mol Cell Biochem* 337: 119–131, 2010.

42. Youdim MB, Edmondson D, and Tipton KF. The therapeutic potential of monoamine oxidase inhibitors. *Nat Rev Neurosci* 7: 295–309, 2006.

43. Zhang D, Mott JL, Farrar P, Ryerse JS, Chang SW, Stevens M, Denniger G, and Zassenhaus HP. Mitochondrial DNA mutations activate the mitochondrial apoptotic pathway and cause dilated cardiomyopathy. *Cardiovasc Res* 57: 147–157, 2003.

Address correspondence to:
Dr. Angelo Parini
INSERM
UMR 1048
Institut des Maladies Métaboliques et Cardiovasculaires
BP 84225
31432 Toulouse Cedex 4
France

E-mail: angelo.parini@inserm.fr

Abbreviations Used

5-HIAA = 5-hydroxyindoleacetic acid
5-HT = 5-hydroxy-tryptamine
Ade = adenovirus
CAT = catalase
Clorg = clorgyline
CoxIV = cytochrome c oxidase IV
DHPG = dihydroxyphenylglycol
DSWT = diastolic septal wall thickness
FS = fractional shortening
GPX = glutathione peroxidase
GSH = glutathione reduced
HF = heart failure
H_2O_2 = hydrogen peroxide
HPLC = high performance liquid chromatography
LDH = lactate dehydrogenase
LV = left ventricle
LVESD = left-ventricular end-systolic diameter
MAO-A = monoamine oxidase-A
MHC = myosin heavy chain
Mn-SOD = superoxide dismutase
MOI = multiplicity of infection
NAC = N-acetyl-cystein
NE = norepinephrine
Ntg = nontransgenic
PGC-1α = peroxisome proliferator-activated receptor-γ coactivator-1α
PWT = posterior wall thickness
ROS = reactive oxygen species
Tg = transgenic
TUNEL = terminal deoxynucleotidyl transferase dUTP nick end labeling